A MECHANISM FOR THE EMERGENCE OF MAGNETIC U-LOOPS AND FLUX CANCELLATION ON THE SUN

T. Magara[1], S. K. Antiochos[2], C. R. DeVore[2], and M. G. Linton[2]

[1]Space Sciences Laboratory, University of California, Berkeley, 94720, United States
[1]Naval Research Laboratory, Washington D.C., 20375, United States
[2]Naval Research Laboratory, Washington D.C., 20375, United States

ABSTRACT

The emergence of U-shaped magnetic field lines (U-loops) is one of the promising scenarios to explain the so-called flux cancellation observed at the solar surface, although the physical mechanism for emerging U-loops is not obvious because plasma tends to accumulate at the dipped part of U-loops, which reduces the buoyancy of these loops. Here we use three-dimensional MHD simulation to investigate the dynamics of emerging U-loops and their possible role in flux cancellation. The simulation reveals that a diverging flow appears around the dipped part of emerging U-loops, which enhances the buoyancy of the loops and helps their emergence into the solar surface. We analyze plasma motions on the field lines related to flux cancellation. We also infer a possible field-line configuration during flux cancellation.

Key words: magnetic fields; MHD; photosphere.

1. INTRODUCTION

Recent observational studies have presented the results that magnetic U-loops play important roles in understanding solar phenomena (van Driel-Gesztelyi, Malherbe, & Démoulin 2000; Bernasconi et al. 2002; Chae et al. 2002 and references therein; Chae, Moon, & Pevtsov 2004; Liu & Kurokawa 2004; Pariat et al. 2004). Flux cancellation is one of those phenomena observed at the solar surface, in which opposite magnetic polarity regions come close together and disappear at the neutral line. There are several scenarios proposed to show the origin of flux cancellation, and the emergence of magnetic U-loops is one of them. The detailed evolution occurring in those scenarios must be examined, and the present study is aimed at the understanding of the dynamics of emerging U-loops and their possible role in flux cancellation. For this purpose, we perform a so-called flux emergence MHD simulation in which magnetic fields evolve through a highly stratified atmosphere extending from the subphotosphere to the corona (Shibata et al. 1989; Yokoyama & Shibata 1996; Matsumoto et al. 1998; Fan 2001; Magara & Longcope 2003; Abbett & Fisher 2003; Magara 2004; Archontis et al. 2004; Manchester et al. 2004; Fan 2004 and references therein; Isobe et al. 2005; Galsgaard et al. 2005). By using this simulation, we investigate the behavior of magnetic fields emerging into the photosphere where flux cancellation is observed, especially focusing on the evolution of U-loops in which plasma tends to accumulate thereby suppressing smooth emergence of the U-loops.

2. NUMERICAL SIMULATION

Figure 1 shows the initial and final states of our ideal MHD simulation using Cartesian coordinates where the z-axis points upward against gravity. As the initial state we assume a hydrostatic atmosphere with an isolated magnetic flux tube inside it. Both the flux tube and the background atmosphere are diffusion-free throughout the simulation, that is, we neglect viscosity, thermal conductivity, radiative transfer, and magnetic resistivity. On the basis of the temperature profile shown in figure 2, the atmosphere stratified under uniform gravity is divided into multiple layers, which are the convection zone ($z < 0$ Mm), photosphere ($z = 0$ Mm), chromosphere (0 Mm $< z <$ 3 Mm), transition region ($z \sim 3.5$ Mm), and corona ($z > 4$ Mm). The temperature gradient in the convection zone is slightly superadiabatic, so this region is weakly unstable against convective motions. The photospheric temperature, gas density, and pressure are given by $T_p = 5000$ K, $\rho_p = 2.42 \times 10^{-7}$ g cm^{-3}, and $P_p = 2 \times 10^5$ dyn cm^{-2}, which define $(\Re T_p/\mu)^{1/2} = 9 \times 10^5$ cm s^{-1}, the photospheric sound speed, and $\Re T_p/(\mu g_p) = 0.3$ Mm, the photospheric pressure scale height (we assume that the gas constant is $\Re = 8.25 \times 10^7$ dyn cm

Proceedings of the International Scientific Conference on Chromospheric and Coronal Magnetic Fields, 30 August – 2 September 2005 (ESA SP-596, November 2005)

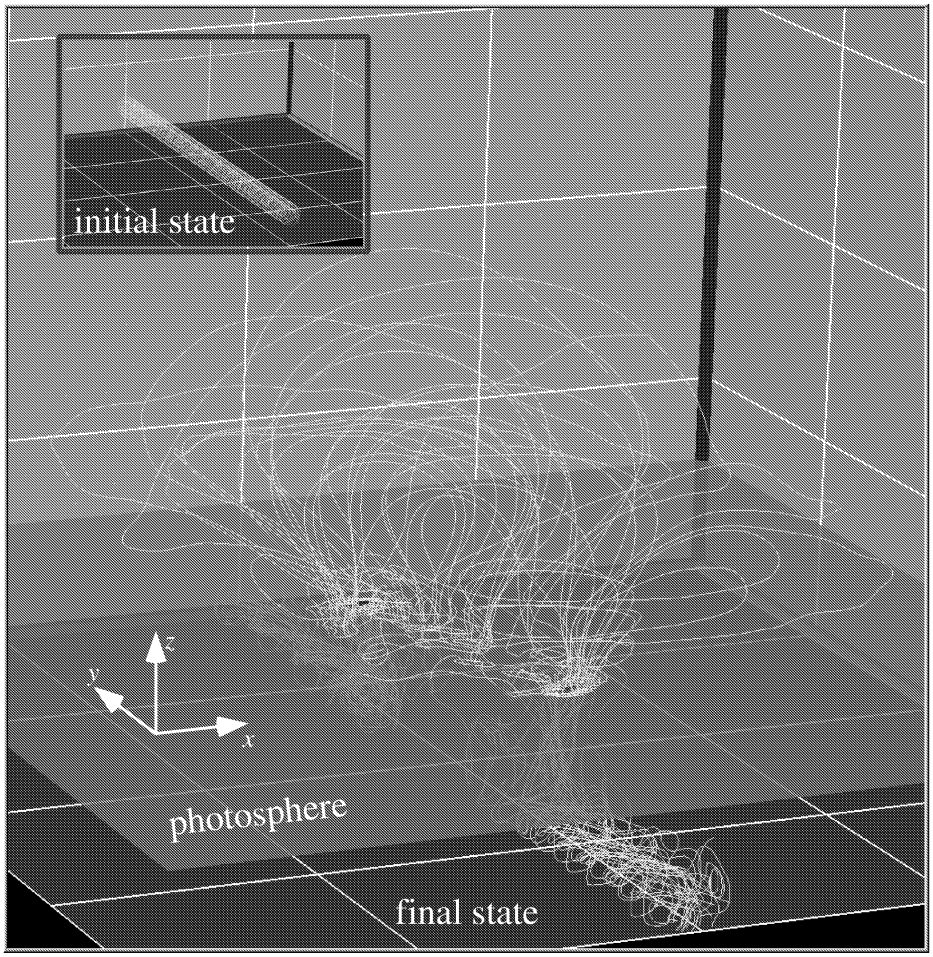

Figure 1. Final state of the simulation. Magnetic field lines (yellow lines) and photospheric vertical magnetic flux (color map) are presented. The initial state is also shown at the top left corner of the figure.

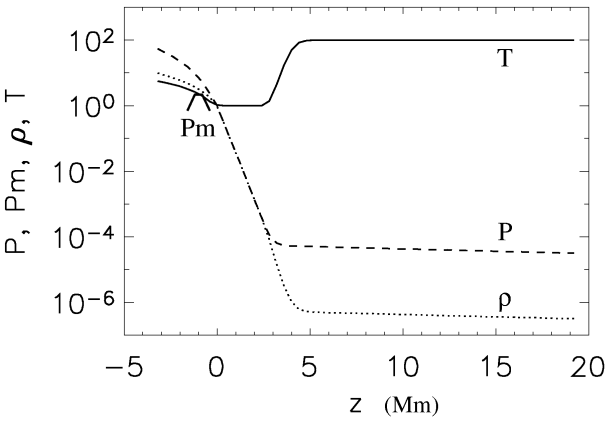

Figure 2. Initial distribution of physical quantities along the z-axis: gas pressure (P), density (ρ), temperature (T), and magnetic pressure (Pm). These quantities are scaled to their photospheric values, and the length is given in Mm.

mol^{-1} K^{-1}, mean molecular weight is $\mu = 0.5$, surface gravity is $g_p = 2.75 \times 10^4$ cm s^{-2}). These values are used to normalize physical quantities in the simulation. Below the photosphere, a straight magnetic flux tube in mechanical equilibrium with the background atmosphere is placed horizontally along the y-axis. The flux tube is composed of twisted field lines that have a Gold-Hoyle profile expressed by

$$\mathbf{B} = B_0 \frac{-b\,(z - z_0)\,\hat{\mathbf{x}} + \hat{\mathbf{y}} + b\,(x - x_0)\,\hat{\mathbf{z}}}{1 + b^2\left[(x - x_0)^2 + (z - z_0)^2\right]} \qquad (1)$$

for $(x - x_0)^2 + (z - z_0)^2 \leq r_f^2$, where $B_0 = 4000$ G is the field strength at the axis of the flux tube, $(x_0, z_0) = (0, -1)$ Mm is the position of the axis in the (x, z)-plane, $r_f = 0.8$ Mm is the radius, and $b = 2.5$ is a parameter characterizing the strength of left-handed twist.

To initiate the simulation we impose an upward flow localized in the middle of the flux tube, and given by:

$$v_z = v_0 \cos\left(\pi \frac{y}{2y_0}\right) \frac{1 - \cos(\pi t / t_0)}{2} \qquad (2)$$

for $(x - x_0)^2 + (z - z_0)^2 \leq r_f^2$, $-y_0 \leq y \leq y_0$, $0 \leq t \leq t_0$, where $v_0 = 5 \times 10^4$ cm s^{-1}, $y_0 = 3.6$ Mm, $t_0 = 10$ s.

The simulation was performed using the Adaptively Refined Mhd Solver (*ARMS*; DeVore et al. 2005). The numerical scheme is a flux-corrected transport method that has second and fourth order accuracy in time and space (DeVore 1991). It solves the nonlinear, time-dependent MHD equations with the parallel adaptive mesh refinement toolkit *PARAMESH* (MacNeice et al. 2000). For the present study, each grid cell is a cube of size (0.1 Mm)^3 below $z = 4.8$ Mm and (0.2 Mm)^3 above that height. The magnetic field gradients in the flux tube were adequately resolved on this grid throughout the simulation, so no dynamic grid adaptation occurred. The total simulation domain is -14.4 Mm $\leq x, y \leq 14.4$ Mm, -3.2 Mm $\leq z \leq 19.2$ Mm. We impose periodic boundary conditions at $y = \pm 14.4$ Mm, free boundary conditions at $x = \pm 14.4$ Mm and $z = 19.2$ Mm, and rigid boundary conditions at $z = -3.2$ Mm.

3. RESULTS

Figure 3 shows a photospheric cut of the partially emerged flux tube at $t = 2200$ s. The contours and colors in this figure represent vertical magnetic flux and κ_B, where

$$\kappa_B \equiv \left(B_x \frac{\partial}{\partial x} + B_y \frac{\partial}{\partial y}\right) B_z \qquad (3)$$

indicates whether magnetic field lines are concave up ($\kappa_B > 0$) or convex up ($\kappa_B < 0$) on the photospheric plane. The regions that satisfy $\kappa_B > 0$ and $B_z = 0$ at the same time are called *bald patches* (Titov et al. 1993) where U-loops are expected to emerge into the photosphere.

Figure 4 shows two selected field lines (red and blue field lines) distributed in the area including such *bald patches*, surrounded by a dashed square in figure 3. These two field lines partially have a U shape, and the dipped part of the red field line is still below the photosphere while the dipped part of the blue field line almost emerges into the photosphere.

Figure 5 shows the velocity and gas pressure distributed along the red and blue field lines. The figure also contains a graph representing how the gas pressure (P), field-aligned component of velocity (v_s), normal component of velocity (v_n), vertical component of velocity (v_z), and divergence of flow ($div\ \mathbf{v}$) are distributed along each of those field lines. In the graph of the red field line v_s changes the sign around $s = s_0$, which means that a diverging flow along the field line occurs around the dip where $div\ \mathbf{v}$ is positive. Taking into account

$$\frac{d\rho}{dt} \equiv \left(\frac{\partial}{\partial t} + \mathbf{v} \cdot \nabla\right) \rho = -\rho\ div\ \mathbf{v} < 0, \qquad (4)$$

and $v_z > 0$ at $s = s_0$, we find that the dipped part of the red field line is in the process of buoyantly emerging into the photosphere. For the blue field line such a diverging flow is less evident (v_s keeps positive around the dip in the graph), although the positive value of $div\ \mathbf{v}$ and v_z at the dip indicates that emergence also proceeds in the blue field line.

Since the simulation domain includes the subphotosphere, it might be interesting to infer a field-line

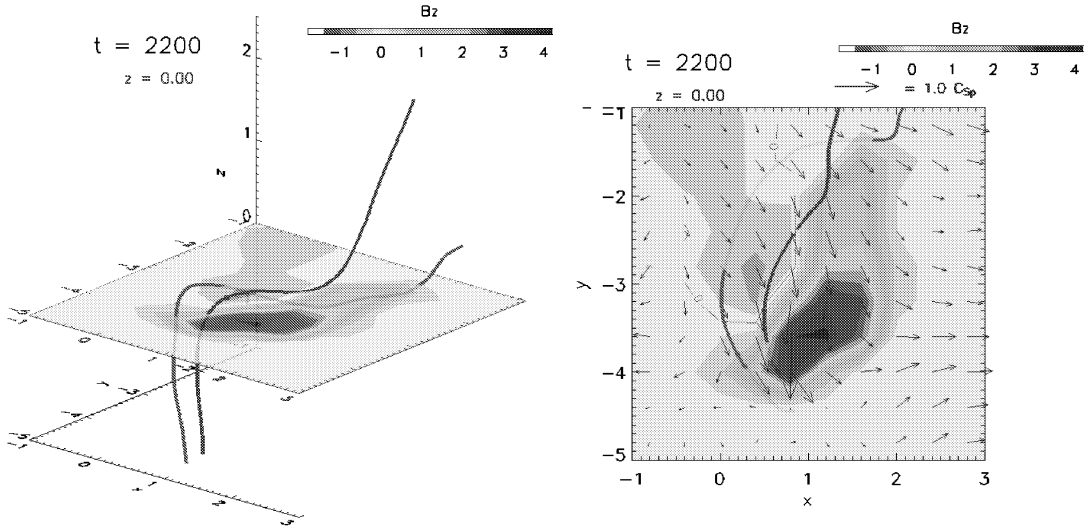

Figure 4. Distribution of U-shaped magnetic field lines (red and blue lines) in the area including bald patches at $t = 2200$ s. Perspective view (left panel) and top view (right panel) are presented. The color map shows photospheric vertical magnetic flux (scaled to 450 G) and arrows in the top-view panel show horizontal velocity (scaled to photospheric sound speed). The length is given in Mm.

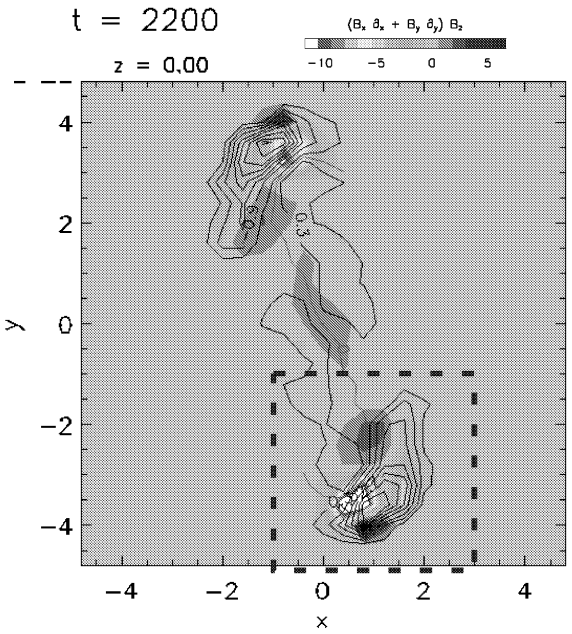

Figure 3. Distribution of photospheric vertical magnetic flux (contours) and κ_B (color map; defined by equation (3)) at $t = 2200$ s. The red line indicates the neutral line. The area surrounded by the dashed square is enlarged in figure 4. The length is given in Mm.

configuration below the photosphere during flux cancellation. In figure 4 the red field line forms two positive poles and one negative pole at the photosphere, and these two positive poles are distributed in the same polarity region (primary polarity region in this area) while the negative pole is located in a satellite polarity region. After the dipped part of the red field line emerges into the photosphere, the negative pole and one of the positive poles will be cancelled (like the way of the blue field line shown in this figure), leaving the other positive pole. This suggests that the satellite polarity region with negative polarity will disappear successively while the primary polarity region with positive polarity remains. We should also point out that we see a relatively simple configuration of photospheric polarity regions in figure 4 although in the real Sun small-scale motions such as granular motions might fragment weak flux areas such as the trails of polarity regions and they are observed as a group of discrete polarity regions.

4. DISCUSSION

The flux cancellation presented here is directly associated to the emergence of a highly twisted flux tube through the photosphere: as both legs of the emerging flux tube become vertical, the distribution of vertical magnetic flux in the photosphere turns to nearly bipolar with a satellite polarity region successively disappearing (flux cancellation). This indicates that the polarity of the axial field of the flux tube is becoming dominant in the photospheric cut at each footpoint.

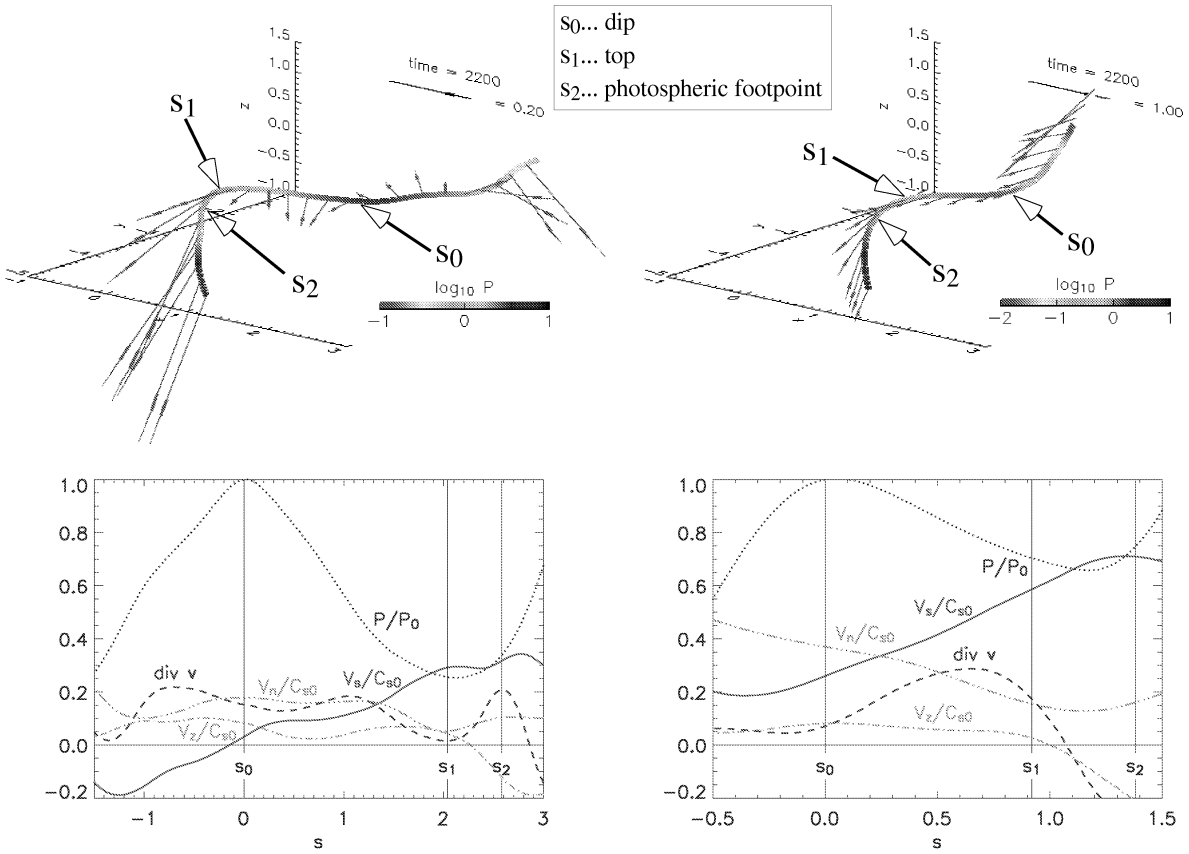

Figure 5. Upper part: Distribution of gas pressure (line colors) and velocity (arrows) along the red (left panel) and blue (right panel) field lines presented in figure 4. The length is given in Mm. Lower part: Distribution of field-aligned component of velocity (v_s), normal component of velocity (v_n), vertical component of velocity (v_z), gas pressure (P), and divergence of flow (div $\mathbf{v}$) along s (distance measured along the red (left graph) and blue (right graph) field lines, scaled to Mm). s_0, s_2, and s_1 are the locations of the dip, the photospheric footpoint, and the highest point between the dip and footpoint, respectively. c_{s0} and P_0 are the adiabatic sound speed and gas pressure at $s = s_0$.

Such emergence of a twisted flux tube causes several key phenomena occurring in the photosphere, apparent flux cancellation and rotational flow, which are believed to have close relations with activities observed in the corona such as coronal mass ejections (CMEs). Apparent flux cancellation occurs between a primary polarity region and a satellite polarity region; a diffuse satellite polarity region (see the orange area in figure 4) is successively absorbed into a primary polarity region (see the violet area in the same figure) while this primary polarity region survives to form one of the main poles in a bipolar region. Such apparent flux cancellation is actually observed in a CME-productive active region (Li et al. 2004). On the other hand, a rotational flow is generated around a primary polarity region and this flow enhances coronal activity by injecting magnetic energy and helicity from the photosphere into the corona (Magara & Longcope 2003). Detailed investigations into how those photospheric phenomena relate with coronal activity are currently in progress (Linker et al. 2003).

It should be mentioned that *bald patches* found in this simulation might be physically important when we study how to form the filament feet called *barbs* (Aulanier & Démoulin 1998). The understanding of the formation of *barbs* will give us some insight into the mechanism of how a cool filament material is supplied to and maintained in the corona.

ACKNOWLEDGMENTS

We wish to thank Dr. J. Luhmann for helpful discussions. T. M. is a member of the Center for Integrated Space Weather Modeling (CISM; ATM-0120950) who collaborates with the NRL on space weather modelling. The numerical simulation presented here has been performed using the ERDC MSRC SGI Origin 3000 Complex. This work is financially supported by NSF, NASA, and ONR.

REFERENCES

Abbett, W. P., & Fisher, G. H. 2003, ApJ, 582, 475

Archontis, V., Moreno-Insertis, F., Galsgaard, K., Hood, A., & OShea, E. 2004, A&A, 426, 1047

Aulanier, G., & Démoulin, P. 1998, A&A, 329, 1125

Bernasconi, P. N., Rust, D. M., Georgoulis, M. K., & Labonte, B. J. 2002, Sol. Phys., 209, 119

Chae, J., Moon, Y., Wang, H., & Yun, H. S. 2002, Sol. Phys., 207, 73

Chae, J., Moon, Y., & Pevtsov, A. A. 2004, ApJ, 602, L65

DeVore, C. R. 1991, J. Comput. Phys., 92, 142

DeVore, C. R., MacNeice, P. J., Olson, K. M.,& Antiochos, S. K. 2005, ApJ, in preparation

Galsgaard, K., Moreno-Insertis, F., Archontis, V., & Hood, A. 2005, ApJ, 618, L153

Fan, Y. 2001, ApJ, 554, L111

Fan, Y. 2004, Living Reviews in Solar Physics, 1, 1

Isobe, H., Miyagoshi, T., Shibata, K., & Yokoyama, T. 2005, Nature, 434, 478

Li, Y., Luhmann, J., Fisher, G., & Welsch, B. 2004, J. of Atm. Solar-Terr. Phys., 66, 1271

Linker, J. A., Mikić, Z., Lionello, R., Riley, P., Amari, T., & Odstrcil, D. 2003, Phys. of Plasmas, 10, 1971

Liu, Y., & Kurokawa, H. ApJ, 610, 1136

MacNeice, P., Olson, K., Mobarry, C., deFainchtein, R., & Packer, C. 2000, Comput. Phys. Commun., 126, 330

Magara, T., & Longcope, D. W. 2003, ApJ, 586, 630

Magara, T. 2004, ApJ, 605, 480

Manchester, W., Gombosi, T., DeZeeuw, D., & Fan, Y. 2004, ApJ, 610, 588

Matsumoto, R., Tajima, T., Chou, W., Okubo, A., & Shibata, K. 1998, ApJ, 493, L43

Pariat, E., Aulanier, G., Schmieder, B., Georgoulis, M. K., Rust, D. M., & Bernasconi, P. N. 2004, ApJ, 614, 1099

Shibata, K., Tajima, T., Steinolfson, R. S., & Matsumoto, R. 1989, ApJ, 345, 584

Titov, V. S., Priest, E. R., & Demoulin, P. 1993, A&A, 276, 564

van Driel-Gesztelyi, L., Malherbe, J.-M., & Démoulin, P. 2000, A&A, 364, 845

Yokoyama, T., & Shibata, K. 1996, PASJ, 48, 353